Spin-Phonon Coupling and Slow-Magnetic Relaxation in Pristine Ferrocenium

Martín Amoza,[a] Lindley Maxwell,[a, b] Núria Aliaga-Alcalde,[c, d] Silvia Gómez-Coca,*[a] and Eliseo Ruiz*[a]

Abstract: We report the spin dynamic properties of non-substituted ferrocenium complexes. Ferrocenium shows a field-induced single-molecule magnet behaviour in DMF solution while cobaltocene lacks slow spin relaxation neither in powder nor in solution. Multireference quantum mechanical calculations give a *non-Aufbau* orbital occupation for ferrocenium with small first excitation energy that agrees with the relatively large measured magnetic anisotropy for a transition metal $S=1/2$ system. The analysis of the spin relaxation shows an important participation of quantum tunnelling, Raman, direct and local-mode mechanisms which depend on temperature and the external field conditions. The calculation of spin-phonon coupling constants for the vibrational modes shows that the first vibrational mode, despite having a low spin-phonon constant, is the most efficient process for the spin relaxation at low temperatures. In such conditions, vibrational modes with higher spin-phonon coupling constants are not populated. Additionally, the vibrational energy of this first mode is in excellent agreement with the experimental fitted value obtained from the local-mode mechanism.

Introduction

Considerable effort by many research groups has been made in the last decades to produce molecular materials that could behave as small nanomagnets (single-molecule magnets, SMMs).[1] Basically, the spin in SMMs has a strong tendency to be aligned in one direction resulting in a behaviour similar to traditional magnets.[2] An additional application of magnetic molecules is to generate qubits as their spin magnetization can be oriented in any space direction.[2–4] For spin qubits magnetic anisotropy is also required but is not as significant as in the SMMs. Usually, the figure of merit for the SMMs is the blocking temperature (below this temperature the system behaves like a magnet) while for qubit molecules is the coherence time (which must be longer than clock time of the quantum computer).[2,4] The molecules with the longest coherence times are mononuclear $S=1/2$ transition metal complexes, usually V^{IV} and Cu^{II} complexes, with moderate/low magnetic anisotropy that also avoid any electronic and/or nuclear spin coupling.[3–6] Recently, titanium cations have been also proposed as qubits[7] or for quantum sensing devices.[8,9] In many cases qubit molecules show field-induced slow spin relaxation, where a small external field suppresses quantum tunnelling of magnetization (QTM) relaxation and the molecular-based material shows slow spin relaxation.

In the field of molecular magnetism, the normal procedure was the use of N- and O-based ligands to coordinate the metals.[10,11] Those studies were also extended to some organometallic systems as well,[12,13] being the $[Fe^{II}(iPr_5C_5)(2,6\text{-}iPr_2C_6H_3)]$ complex one of the first reported mononuclear transition metal SMM.[14] Regarding metallocene complexes, those with Dy^{III} ions are especially remarkable as they show the highest blocking temperature (open hysteresis) among the SMM compounds to date.[15,16] Herein, we want to focus on the ferrocenium molecule, one of the most studied families in organometallics. Static magnetic susceptibility,[17,18] EPR[19,20] and Mossbauer[21–25] experiments have been employed to analyze the ground state of ferrocenium which was found to be $^2E_{2g}$ $[(a_{1g})^2(e_{2g})^3]$. The relative energy order of the a_{1g} and e_{2g} orbitals, and consequently the *Aufbau* or *non-Aufbau* configuration of ferrocenium, it was also a controversy from the first papers of the neutral ferrocene molecule.[26,27] Recently, some of us have reported a study of the magnetic properties of some substituted ferrocenium molecules showing slow spin relaxation.[28]

[a] Dr. M. Amoza, Dr. L. Maxwell, Dr. S. Gómez-Coca, Prof. E. Ruiz
Departament de Química Inorgànica i Orgànica and
Institut de Recerca de Química Teòrica i Computacional
Universitat de Barcelona
Diagonal 645, 08028 Barcelona (Spain)
E-mail: silvia.gomez@qi.ub.es
eliseo.ruiz@qi.ub.es

[b] Dr. L. Maxwell
Advanced Lithium and Industrial Minerals Research Center
Universidad de Antofagasta
Av. Universidad de Antofagasta, 02800 Antofagasta (Chile)

[c] Prof. N. Aliaga-Alcalde
ICREA, Institució Catalana de Recerca i Estudis Avançats
Passeig, Passeig Lluis Companys 23, 08010 Barcelona (Spain)

[d] Prof. N. Aliaga-Alcalde
Institut de Ciència de Materials de Barcelona
ICMAB-CSIC, Campus UAB, 08193 Bellaterra, Catalonia (Spain)

Supporting information for this article is available on the WWW under https://doi.org/10.1002/chem.202102603

The analysis of the experimental dynamic susceptibility allows to determine the main spin relaxation mechanism of the spin-lattice contribution (usually quantified using T_1 or τ). However, the goal of this work is to provide insight into the spin relaxation processes of non-substituted magnetic $S=1/2$ metallocene molecules, ferrocenium and cobaltocene, especially focusing on the role of the spin-phonon relaxation mechanism and the link between theory and experiments.[29]

The usual way of quantifying magnetic anisotropy in single molecule magnets (for systems with $S>1/2$) is by the D value, zero-field splitting (ZFS), and the diagonal components of the g tensor.[30–32] The D and g values can be determined with the expressions that depend on the low-lying energy excitations. Hence, the orbitals involved in the electronic excitation will have significant contributions to the k-integrals with the k-component of the angular momentum operator. The calculation of the ZFS parameters was previously discussed[31,32] and similar expression for the g components can be obtained [Eq. (1)]:

$$g_{kl}=g_e+\frac{\zeta_{eff}}{2S}\sum_{i,p}\frac{\langle\varphi_i|l_k|\varphi_p\rangle\langle\varphi_p|l_l|\varphi_i\rangle}{\varepsilon_p-\varepsilon_i}-\frac{\zeta_{eff}}{2S}\sum_{p,a}\frac{\langle\varphi_p|l_k|\varphi_a\rangle\langle\varphi_a|l_l|\varphi_p\rangle}{\varepsilon_a-\varepsilon_p} \quad (1)$$

where ζ_{eff} is the spin-orbital coupling constant, l_k is the k-component of the angular momentum operator and φ are the molecular orbitals (with orbital energies ε) with the subindex i, p or a to indicate double-occupied, singly-occupied or empty orbitals, respectively. The "textbook" orbital splitting of the d orbitals of the ferrocene molecule is show in Figure 1.

In such electronic structure, the oxidized form of ferrocene, ferrocenium, should have an unpaired electron in the d_z2 orbital. The excitations that provide effective contributions (considering non-zero angular momentum integrals) are those involving transition from the SOMO d_z2 orbital to the empty d_{xz} and d_{yz} orbitals, providing low magnetic anisotropy values. However, for the d^7 cobaltocene the unpaired electron should be placed in one of the close to degeneracy d_{xz} and d_{yz} orbitals; the excitations involving these two orbitals should result in large anisotropy values. In this communication, we studied, using SQUID measurements, the magnetic properties of non-substituted ferrocenium and cobaltocene molecules. Considering the above premises, we present unexpected results, showing ferrocenium field-induced SMM behaviour and lacking cobaltocene of SMM features, for which we provide a rational explanation for the observed behaviour. Additionally, a proper description of the role of the spin-phonon coupling in the spin relaxation of these ferrocenium is presented showing its relevance in the spin relaxation.

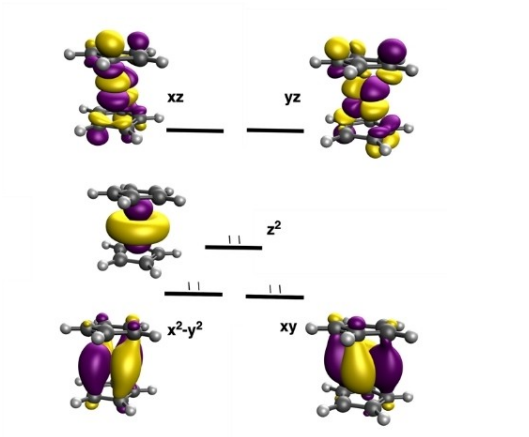

Figure 1. "Textbook" orbital splitting of the d orbitals in the ferrocene molecule.[33]

Experimental Section

Magnetic susceptibility measurements

Susceptibility measurements (direct (DC) and alternating (AC) current) were carried out with a Quantum Design SQUID MPMS device. Static susceptibility measurements were carried out between 2 and 300 K with an applied DC field of 1000 G. An oscillating *ac* field of 4 Oe was used in the AC measurements together with frequencies ranging from 1 to 1500 Hz and the external DC field indicated. Polycrystalline samples were grinded and introduced in a gelatine capsule that was mounted in a capillary tube made of polyimide. Different samples were measured, and the quantities oscillate between 30 and 50 mg. Solution samples were prepared by dissolving around 10 mg of the solid in biotechnological grade DMF in around 100–200 mg and sonicating the mixture in a bath. The solution was sealed in a tube of polyimide and immediately after introduced in the MPMS device. The cobaltocene solid sample and solution samples were prepared under Argon atmosphere. For the capsule and DMF blank measurements were performed and their diamagnetic contribution corrected. Diamagnetic corrections for the measured compounds were estimated from Pascal Tables.

Computational details

To give some insights about the unexpected magnetic behaviour of the studied metallocene molecules, theoretical calculations were performed with CASPT2 or NEVPT2 methods. Two software packages were employed, MOLCAS (8.0 version, ANO-RCC basis set with [6 s5p4d2 f] for Fe and Co, [4 s3p1d] for C and [2 s] for H contractions)[34,35] and Orca (4.0.1.2 version, def2-TZVP basis set) codes.[36] The results with both programs are consistent and the small differences are due to the different basis set and some minor alternatives in the theoretical approaches. Different experimental and symmetric structures as well as different active spaces were studied,[37,38] see Supporting Information for details. Although the effect of the active space has been studied the active space with only the five d orbitals was selected for the main discussion because it provides the right multiplicity for the ground state at NEVPT2 level (CASSCF provides a wrong $S=5/2$ spin value of the ground state with such active space) and also, it allows to analyse the orbitals with the AILFT (Ab initio Ligand Field Theory) approach.[39]

The calculation of the vibrational frequencies was performed using Gaussian09 code[40] with the B3LYP functional[41] using a TZVP basis for iron atoms and lighter atoms were described using the QZVP basis set.[42,43] The calculation of the spin-phonon coupling for the first 31 lowest vibrational modes was done with the NEVPT2

approach implemented in the Orca code using the vibrational modes calculated with DFT making shifts until the range ±0.8 Å with steps of 0.2 Å.

Results and Discussion

Magnetic characterization

The DC magnetic data for ferrocenium agrees with a $S=1/2$ ion, low spin Fe^{III},[18,44] with a considerable spin-orbit coupling, Figure S1. The χT value at 300 K is 0.98 $cm^3\,K\,mol^{-1}$, larger than the expected (0.375) for a spin-only $S=1/2$ system. When decreasing temperature χT product decreases in a linear way until 100 K and rapidly afterwards, down to a value of 0.69 $cm^3\,K\,mol^{-1}$ at 2 K. The magnetization achieves 1.21 μ_B at 5 T and it could be fitted to a Brillouin function with an average g value of 2.6. These results indicate a large anisotropy of the molecule. In the case of cobaltocene,[45,46] the χT value at 300 K is 0.376 $cm^3\,K\,mol^{-1}$, expected value for a spin-only $S=1/2$ system, Figure S2. The χT product decreases with temperature to a value of 0.262 $cm^3\,K\,mol^{-1}$ at 8 K and slightly increases afterwards. The magnetization achieves 0.72 μ_B at 5 T and it could be fitted to a Brillouin function with an average g value of 1.7, indicating small anisotropy for the molecule. The data agreed with similar systems and previous published data;[45,46] and it also concords with the results of the calculations, see below.

The AC magnetic susceptibility of $[CoCp_2]$ in the solid state and in solution at low temperatures was investigated under the absence and presence of external DC fields, however in all the cases no out-of-phase signals were observed (see Figures S3 and S4). On the other hand, the ferrocenium complex $[FeCp_2]PF_6$ shows a frequency dependence of χ''_M with an external field either in solid samples (see Figures S5 and S7) or in DMF solutions (see Figure 2). The frozen solution sample shows slower spin relaxation than the solid one. It is probably due to the decrease of the tunnelling contribution which depends on the dilution of the sample, where the most diluted samples present smaller magnetic dipolar interactions and consequently, less efficient tunnelling relaxation.[47] The spin-lattice relaxation rate parameter τ was determined, at each given DC magnetic field and temperature, by fitting the Cole-Cole plots to a Debye function using the CC-FIT program (see Supporting Information).[48] For the solid sample, field dependence was measured at 2 K and temperature dependence at 5000 Oe. However, the maxima of the curves are very close to the maximum frequency value we can employ in our SQUID magnetometer and therefore the maxima were only observed for a couple of fields and temperatures. In addition, the curves displayed at least two processes and the α values obtained from the fit (Tables S1–S3) show a wide distribution of relaxation times. In view of these results, no further analysis was done using the solid sample data.

For the DMF ferrocenium solution, field dependence AC measurements were acquired at 2 K and temperature dependence was measured at 500 Oe, Figure 2. The results from the fit

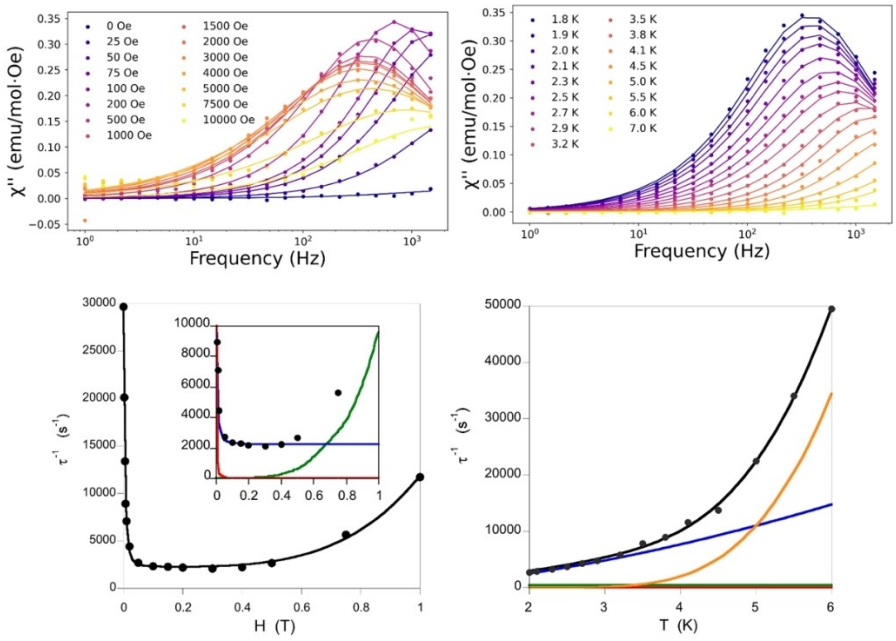

Figure 2. Imaginary susceptibility versus frequency at (top left) 2 K and different external fields and (top right) at 500 Oe external DC field and different temperatures of $[FeCp_2]PF_6$ complex in DMF solution. Lines are the result of the fit using the CC-FIT program. (bottom left) Plot of τ^{-1} versus field for the $[FeCp_2]PF_6$ complex in DMF solution. (bottom right) Plot of τ^{-1} versus T for the $[FeCp_2]PF_6$ complex in DMF solution. The black solid line represents the fit of the experimental data (black dots) with the terms of Equations (3) and (4), respectively. In the inset of the field dependence, green, blue and red lines correspond to the direct, Raman and tunnelling contributions. In the temperature dependence (right), green, blue, red and orange lines correspond to the direct, Raman, tunnelling and local mode contributions.

with the Cole-Cole expressions using the CC-FIT program.[48] and the Cole-Cole diagrams are available in the Supporting Information (Tables S4 and S5). Using the obtained τ values, the spin relaxation mechanism can be studied by analysing the dependence of τ^{-1} with T and the magnetic field using the following equation [Eq. (2)]:[49]

$$\tau^{-1} = aH^4T + \frac{B_1}{1+B_2H^2} + d\left(\frac{1+eH^2}{1+fH^2}\right)T^n + C\left(\frac{e^{-\omega/T}}{(e^{-\omega/T}-1)^2}\right) \quad (2)$$

The terms in Equation (2) refer to direct relaxation, tunnelling, field-dependent Raman and local-mode relaxation mechanisms, in that order. Here, Orbach phenomena were not considered due to the $S=1/2$ nature of our system, lacking three states to define an energy barrier. The Raman term is a field-dependent term using the Brons-van Vleck equation,[50] it has a field dependent prefactor and also the typical exponential dependence with the temperature. In the field-dependent Raman term, the d parameter corresponds to the zero-field relaxation (equivalent to the tunnelling rate in systems with higher spin values), the e parameter strongly depends on the paramagnetic centres concentration and introduces the relaxation of the interacting spins; finally, the f parameter accounts the effect of the external field to suppress the spin relaxation. Usually, such field-dependent Raman expression was only employed in $S=1/2$ systems despite that the original van Vleck's paper was devoted to $S=1/2$ and $S=3/2$ compounds.[50] The local-mode term[51] directly relates to the spin-phonon coupling of the vibrational modes of the molecule, ω in K units in Equations (2) and (4), and this relaxation mechanism is not included in the other three terms. Thus, the spin relaxation is promoted through an excited vibrational state of the electronic ground state and depends exclusively on the applied temperature to increase the population of the excited vibrational state [Eq. (3)].

$$\tau^{-1} = aH^4T + \frac{B_1}{1+B_2H^2} + d\left(\frac{1+eH^2}{1+fH^2}\right)T^n \quad (3)$$

The fitting of the τ^{-1} versus field and temperature dependence is a difficult task, due to the large number of parameters in Equation (2). However, the analysis of the τ^{-1} with the field dependent terms using Equation (3) shows that there are three regions (also noticed in lanthanide systems[52]): i) the high-field region, clearly governed by the H^4 term of the direct contribution; ii) the low-field region, controlled by the quantum tunnelling term which decreases the τ^{-1} value, breaking the degeneracy of the ground state; and finally, iii) the intermediate region, where the field-dependent Raman contribution is the dominant term. The local-mode term was not included in this fit as it will be constant with the applied DC field and it is expected to have a very small value at the experiment temperature. Thus, each region was independently fitted (0–0.05, 0.05–0.4 and 0.4–1 T) with the corresponding terms, and the obtained set of parameters was employed as starting point for the fitting of the whole set of data [Eq. (3)]. The obtained final values were $a=4800\ s^{-1}\ T^{-4}\ K^{-1}$, $B_1=17692\ s^{-1}$, $B_2=151340\ T^{-2}$, $dT^n=11967\ s^{-1}$, $e=2819\ T^{-2}$ and $f=15085\ T^{-2}$. Following such procedure, the parameters obtained in the previous fit were fixed and the curve of τ^{-1} versus temperature was fitted allowing the variation of only three parameters (Eq. (4)): the n exponent of the Raman term and the two parameters of the local-mode relaxation. Obtained fit values are, $n=1.62$, $C=1.034\times10^7\ s^{-1}$ and $\omega=34.2$ K (23.7 cm^{-1}).

$$\tau^{-1} = A(H)T + K(H) + D(H)T^n + C\left(\frac{e^{-\omega/T}}{(e^{-\omega/T}-1)^2}\right) \quad (4)$$

In the temperature dependence fitting, the direct term is almost negligible due to the low employed magnetic field, like the constant tunnelling contribution (see Figure 4). The n exponent of the Raman term is relatively low, but similar to other $S=1/2$ mononuclear complexes.[28,53] Although the Raman and local-mode terms have different dependence with temperature, the curves are quite similar and the inclusion of the local-mode term reduces the obtained n value. At low temperatures the local-mode term has a very small value (as it was expected), however it becomes very important at high temperatures due to the participation of additional vibrational modes in the spin relaxation. The importance of the local-mode has been already noticed in many experimental papers providing a fitting of the experimental data.[54,55] However, in the next section we want to stress the correlation between the fitted frequency and the ab initio calculated spin-phonon coupling constants.

Electronic structure calculations

In this section, the goal is to use CASSCF-type calculations to determine the origin of the magnetic anisotropy in the studied $S=1/2$ metallocene systems and also, to calculate the spin-phonon parameters of the ferrocenium molecule to analyse which are the vibrational modes that can induce the spin relaxation.

To corroborate the accuracy of the theoretical description of the magnetic properties of both systems, we provide the comparison between theoretical and experimental χT versus T and M versus H curves for ferrocenium (Figures S1 and S2). Different experimental structures[56–58] (see Section S3.1, for the reported systems in the Cambridge Structural Database[59,60]) were calculated with a (5,5) active space and the results show a strong dependence with the employed structures (Table S6). The calculated g_i components at CASPT2-RASSI level are $g_z=5.94$ and $g_x=g_y=0.02$ with the z direction aligned perpendicular to the Cp rings for the KEXKOU08_A system[58] and slightly higher than those obtained at NEVPT2 level (g_z around 5.7), see Table S6 and Figure S15. The degree of distortion of the five calculated ferrocenium molecules has been analysed with the help of the Shape code[61,62] (Table S6). These results show that small distortions have a great impact on the g values. Thus, the two KEFXUO molecules with a relatively small distortion (Shape values 0.10 and 0.14 from the staggered non-distorted molecule) have a calculate g_z value around 3.3 while for the two almost staggered molecules (KEFXUO01_A1 and KEFXUO08_A

Shape values 0.01 and 0.02) the g_z values are around 5.7. Thus, the experimental values[19] ($g_z = 4.35$ and $g_x = g_y = 1.30$) seem an average of the calculated values for the experimental structures or that corresponding to an intermediate structure. The NEVPT2 spin-orbit coupling for the KEFXUO08_A system is $\zeta = 399\ cm^{-1}$. The ζ_0 value for a Fe^{III} low-spin is not usually reported in the set of spin-orbit values as they focused on high-spin systems. Thus, we have calculated the Fe^{III} cation by using the same approach than for the molecule (NEVPT2) and the ζ_0 value is $470\ cm^{-1}$. The calculated covalent orbital reduction factor is $k = 0.84$ in nice agreement with that proposed by Prins, $k = 0.82$, for a family of ferrocenium molecules.[19]

Additionally, the effect of the active space was tested as it can be important to enlarge the active space in some transition metal complexes, especially in Fe^{III} compounds (see Table S7). Virtual and double occupied orbitals were included in the active space, see Supporting Information. The calculated energy spectra, Figure S16, relative energy of the first excited KDs, see Table S8, and g factors of the ground KDs, Table S9, show that the inclusion of occupied orbitals in the active space gives to the correct ground state even at CASSCF level of theory. In all the cases at NEVPT2 level of theory similar the ground and first excited states are doublets with similar relative energies. Hence, the (5,5) active space at NEVPT2 or CASPT2 level of theory gives a proper description of the system and allows to analyse the orbitals with the AILFT approach.

The origin of the easy-axis anisotropy can be understood taking into account that the *non-Aufbau* ground state of ferrocenium corresponds to a $d_x2_{-y}2^2\ d_{xy}^1\ d_z2^2$ orbital occupation (a similar case was found in a Co^{II} linear complex).[63] The different interelectronic repulsion of such orbitals is enough to compensate their energy difference, resulting in an anomalous occupation. According to Equation (1), the low-energy excitation, from the doubly-occupied $d_x2_{-y}2$ to singly-occupied d_{xy} orbital, results in a large positive g_z contribution, as the one found in the CASPT2/NEVPT2 calculations, agreeing with the easy-axis anisotropy found experimentally and showing a similar behaviour as substituted ferrocenium and Fe^{III} carborane compounds.[28,64] Furthermore, the ground state has a strong multireference character after the inclusion of spin-orbit coupling. At CASSCF level, the two involved electronic configurations ($d_x2_{-y}2^2d_{xy}^1d_z2^2$ and $d_{xy}^2d_x2_{-y}2^1d_z2^2$) have a weight each close to one in the first two states. There is no mixing because there is only one electron difference while interelectronic repulsion is a two-electron operator but the inclusion of the spin-orbit coupling results in a 50–50 mixing of the two first CASSCF roots (see Section S3.3, Tables S10–S13). It is also worth noting the large dependence of the orbital energy splitting at AILFT level with the structure employed in the calculations (Table S14), like the changes in the *g* values discussed above.

For cobaltocene, the CASPT2-RASSI calculations give a picture close to an easy-plane anisotropy with $g_z = 1.27$, $g_x = 2.07$ and $g_y = 1.86$ with the *xy* plane parallel to the Cp rings but the anisotropy is rather low, confirming the absence of SMM behaviour found experimentally. The orbital occupation for the d^7 cobaltocene ($d_z2^2\ d_x2_{-y}2^2\ d_{xy}^2\ d_{xz}^1\ d_{yz}^0$) must present a Jahn-Teller distortion as the ferrocenium but the degenerate orbitals involved (d_{xz}, d_{yz}) have larger antibonding character for the case of the cobaltocene molecule than for the ferrocenium ($d_x2_{-y}2$, d_{xy}). Thus, the energy gap between the two degenerate orbitals caused by the distortion (see AILFT orbital energies in Table S14) can be compared in value with the first excitation energy before the inclusion of the spin-orbit effect; the calculated values at CASPT2/NEVPT2 levels are around 300 and 1200 cm^{-1} for ferrocenium and cobaltocene, respectively. These two values clearly indicate the magnitude of the spin-orbit contributions, being much larger for ferrocenium, and justifying the larger magnetic anisotropy determined experimentally for such system in comparison with the cobaltocene.

The spin relaxation mechanisms in the ferrocenium system extracted from the CASPT2 calculation are summarized in Figure 3. The first excited state is over $800\ cm^{-1}$ being the thermal process disregarded. An important quantum tunnelling through the Kramers doublet ground state is noticed, being the dominating spin relaxation mechanism at low temperatures and at zero external field. The relatively large QTM, in the doublet ground state, agrees with the experimental fitting obtained with Equation (3), where such mechanism is predominant at low external fields. Furthermore, the analysis of the spin relaxation mechanisms of cobaltocene (see Figure S17) shows a large QTM, in the ground state, that cannot be overcome with the applied static field (to reach slow spin relaxation) and therefore unreachable with the SQUID measurements in contrast to what is observed for the ferrocenium system.

The role of the spin-phonon coupling in the spin relaxation has been extensively discussed during the last years using

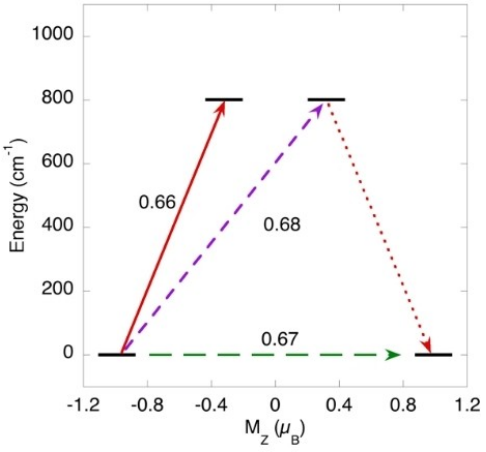

Figure 3. Lowest two Kramers doublets and ab initio computed relaxation mechanism with the MOLCAS code (CASPT2 + RASSI level) for the ferrocenium molecule. The thick black lines imply KDs as a function of their magnetic moment, M_z, along the main anisotropy axis (*z*). Red lines indicate the magnetization reversal mechanism. The green lines correspond to QTM in the ground state KDs in zero-field relaxation mechanism, while purple and red lines show the hypothetical thermally activated relaxation processes. The values close to the arrows indicate the matrix elements of the transition magnetic moments (above 0.1, an efficient spin relaxation mechanism is expected). This figure indicates that spin relaxation through the QTM in the Kramers doublet ground state is dominating the relaxation process at low temperatures and zero external field.

different approaches[15,29,65–70] (see also some recent reviews[2,4,33]). The spin phonon term for each vibrational mode C_k [see Eq. (5)] can be calculated using Equation (5) as the second derivative of the g_z component with the structural distortion coordinate Q_k associated to the vibrational mode k,[29,68]

$$C_k = \frac{\hbar}{4\pi}\left(\frac{\partial^2 g_z}{\partial Q_k^2}\right)\frac{1}{m_k \nu_k} \quad (5)$$

$m_k\upsilon_k$ is the product of the reduced mass and frequency for the k vibrational mode. To include the effect of the thermal population of the vibrational modes, the magnitude B_k was defined with the help of Bose-Einstein statistics [Eq. (6)]:

$$B_k = \frac{C_k}{e^{\nu_k/k_B T}-1} \quad (6)$$

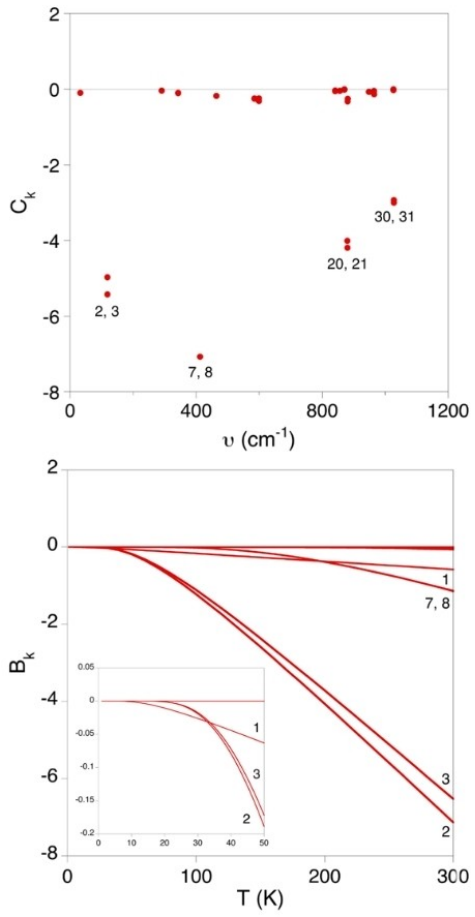

Figure 4. Calculated C_k and B_k values spin-phonon constants for each vibrational k mode calculated at NEVPT2 level for the vibrational modes calculated at DFT level with the B3LYP functional for the vibrational modes under the first electronic excitation. The inset in the B_k dependence was included to visualize the main role of the first vibrational mode at low temperatures.

The calculated C_k and B_k values are collected in Figure 4 (see Computational details for the employed theoretical methods).

The first vibrational mode and the vibrational modes with largest spin phonon coupling C_k are described in Figure 5. They involve changes in the relative energy of the $d_{x^2-y^2}$ and d_{xy} orbitals that result, as we have previously discussed, in larger variations of the g_z component (see Figure S18 and Table S15). To compare such results with the experimental data, the analysis of the dependence of the spin relaxation time with the temperature was performed at 2 K. Thus, as we can see in the inset (variation of B_k values with the temperature, Figure 4), despite a relatively small C_k spin-phonon coupling, the first vibrational mode is predominant until 30 K. Hence, the other modes, with larger spin-phonon couplings, are not efficient for the spin relaxation at low temperature because their populations are too small. Mode 1 has a calculated energy at B3LYP level of 32.3 cm^{-1} in nice agreement with the extracted value for the fitted ω parameter of the local-mode term [see Eq. (4), 23.7 cm^{-1}]. This result is remarkable because it allows to link the mathematical expression proposed for the local-mode term in the fitting of the experimental temperature dependence of the relaxation time with the ab initio spin-phonon calculations.

Conclusion

The magnetic properties of non-substituted ferrocenium and cobaltocene compounds have been explored using experimental and theoretical methods. The ferrocenium complex show a remarkable slow-spin relaxation due to a *non-Aufbau* occupation of the molecular orbitals, resulting in a relatively large magnetic anisotropy. In frozen DMF solution, the complete analysis of the relaxation time was performed taking advantage of the fact that the spin dilution diminishes the efficiency of the quantum tunnelling relaxation. Cobaltocene does not present slow-spin relaxation neither in powder nor in solution because the orbitals involved in the lowest energy transitions have

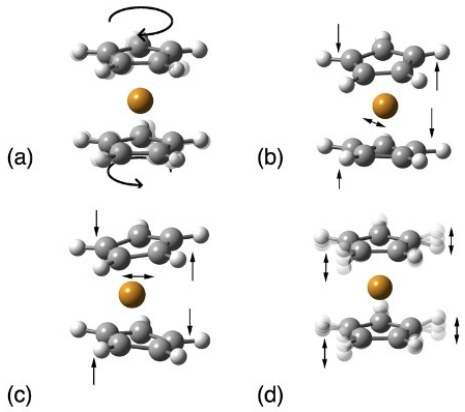

Figure 5. Vibrational modes of $[FeCp_2]^+$ with the largest spin-phonon couplings (see Figure 4): (a) mode 1; (b) mode 2 degenerated with equivalent mode 3; (c) mode 7 with equivalent degenerated mode 8; (d) mode 20 degenerated with equivalent to mode 21.

antibonding character. Thus, the Jahn-Teller distortion in this molecule causes a relatively large energy splitting in comparison with the ferrocenium system,[71–74] that have mostly non-bonding character. Such large excitation energies of cobaltocene results in a small magnetic anisotropy.

The analysis of the spin relaxation for ferrocenium species shows that different spin relaxation mechanisms are important depending on temperature and external field conditions. At low temperature, quantum tunnelling mechanism leads at low fields, Raman mechanism does for intermediate fields and the direct term becomes predominant at high fields. The temperature dependence shows that Raman and local-mode terms have non-negligible contributions in the whole temperature range studied. Concerning the local-mode spin relaxation, the fitted frequency obtained from the experimental data is in good agreement with the theoretical analysis of the spin-phonon coupling values for each vibrational mode. It is worth to remark that despite there are vibrational modes with larger spin-phonon coupling values, the most efficient mode to produce the spin relaxation, is the first vibrational mode (around 25 cm^{-1}), besides its low spin-phonon coupling. This agrees with the experimental data and it is a consequence that at low temperatures, higher energy vibrational modes with the largest spin-phonon coupling constants are not populated and therefore, they are not involved in the spin relaxation. Finally, we want to highlight the importance of the local-mode relaxation mechanism that it is usually not considered in most of the analysis. In conclusion, ferrocenium is a promising system with medium-high magnetic anisotropy, easy spin dilution with solvents or cobaltocenium analogues (small spin-spin relaxation), with the magnetic orbitals free of non-zero nuclear atoms, that is, hydrogen atoms, thus, hyperfine effects should be non-important in the spin relaxation. And further investigations are being conducted on these directions.

Supporting Information

Static magnetic measurements of $[FeCp_2]PF_6$ and $[CoCp_2]$, dynamic magnetic measurements of $[FeCp_2]PF_6$ and additional computational results (calculations of experimental structures, active space calculations, calculated AILFT energies and spin-phonon coupling constants).

Acknowledgements

The research reported here was supported by the Spanish Ministerio de Ciencia, Innovación y Universidades (grants PGC2018-093863-B-C21, PID2019-108794GB-I00 and centres of excellence MDM-2017-0767 and Severo Ochoa FUNFUTURE (CEX2019-000917-S). E.R. thanks Generalitat de Catalunya for an ICREA Academia award and for the SGR2017-1289 and -1277 grants. S.G.-C. thanks the Generalitat de Catalunya for a Beatriu de Pinòs grant. M.A. acknowledges the Ministerio de Educación, Cultura y Deporte for an FPU predoctoral grant. Authors acknowledge computer resources, technical expertise and assistance provided by the CSUC. We want to thank Prof. Santiago Alvarez for his help with the Shape code.

Conflict of Interest

The authors declare no conflict of interest.

Keywords: ab initio calculations · magnetic properties · metallocenes · spin dynamics · spin-phonon coupling

[1] D. Gatteschi, R. Sessoli and J. Villain, Molecular Nanomagnets, Oxford University Press, Oxford, **2006**.
[2] E. Coronado, *Nat. Rev. Mater.* **2020**, *5*, 87–104.
[3] J. M. Zadrozny, J. Niklas, O. G. Poluektov, D. E. Freedman, *ACS Cent. Sci.* **2015**, *1*, 488–492.
[4] M. Atzori, R. Sessoli, *J. Am. Chem. Soc.* **2019**, *141*, 11339–11352.
[5] S. Sproules *Molecules as electron spin qubits, in Electron Paramagnetic Resonance Vol. 25* (Eds.: V. Chechik and D. M. Murphy), **2017**, pp. 61.
[6] S. K. Jain, C.-J. Yu, C. B. Wilson, T. Tabassum, D. E. Freedman, S. Han, *Chem* **2021**, *7*, 421–435.
[7] L. C. de Camargo, M. Briganti, F. S. Santana, D. Stinghen, R. R. Ribeiro, G. G. Nunes, J. F. Soares, E. Salvadori, M. Chiesa, S. Benci, R. Torre, L. Sorace, F. Totti, R. Sessoli, *Angew. Chem. Int. Ed.* **2021**, *60*, 2588–2593. *Angew. Chem.* **2021**, *133*, 2620–2625.
[8] C.-J. Yu, S. von Kugelgen, D. W. Laorenza, D. E. Freedman, *ACS Cent. Sci.* **2021**, *7*, 712–723.
[9] K. A. Collins, D. E. Freedman, *Nat. Chem.* **2020**, *12*, 670–671.
[10] D. Gatteschi and C. Benelli, *Introduction to Molecular Magnetism: from Transition Metals to Lanthanides*, Wiley-VCH, Weinheim, **2015**.
[11] B. Sieklucka and D. Pinkowicz, *Molecular Magnetic Materials: Concepts and Applications*, Wiley-VCH, **2017**.
[12] R. A. Layfield, *Organometallics* **2014**, *33*, 1084–1099.
[13] D. N. Woodruff, R. E. P. Winpenny, R. A. Layfield, *Chem. Rev.* **2013**, *113*, 5110–5148.
[14] D. Weismann, Y. Sun, Y. Lan, G. Wolmershäuser, A. K. Powell, H. Sitzmann, *Chem. Eur. J.* **2011**, *17*, 4700–4704.
[15] C. A. P. Goodwin, F. Ortu, D. Reta, N. F. Chilton, D. P. Mills, *Nature* **2017**, *548*, 439–442.
[16] F.-S. Guo, B. M. Day, Y.-C. Chen, M.-L. Tong, A. Mansikkamäki, R. A. Layfield, *Science* **2018**, *362*, 1400–1403.
[17] D. N. Hendrickson, Y. S. Sohn, H. B. Gray, *Inorg. Chem.* **1971**, *10*, 1559–1563.
[18] Y. S. Sohn, D. N. Hendrickson, H. B. Gray, *J. Am. Chem. Soc.* **1970**, *92*, 3233–3234.
[19] R. Prins, *Mol. Phys.* **1970**, *19*, 603–620.
[20] R. Prins, F. J. Reinders, *J. Am. Chem. Soc.* **1969**, *91*, 4929–4931.
[21] M. Abraham, H. H. Klauß, W. Wagener, F. J. Litterst, A. Hofmann, M. Herberhold, *Hyperfine Interact.* **1999**, *120/121*, 253–256.
[22] R. H. Herber, I. Felner, I. Nowik, *Hyperfine Interact.* **2016**, *237*.
[23] I. Nowik, R. H. Herber, *Inorg. Chim. Acta* **2000**, *310*, 191–195.
[24] H. Schottenberger, K. Wurst, U. J. Griesser, R. K. R. Jetti, G. Laus, R. H. Herber, I. Nowik, *J. Am. Chem. Soc.* **2005**, *127*, 6795–6801.
[25] M. Reiners, D. Baabe, P. Schweyen, M. Freytag, P. G. Jones, M. D. Walter, *Eur. J. Inorg. Chem.* **2016**, *2017*, 388–400.
[26] H. H. Jaffé, *J. Chem. Phys.* **1953**, *21*, 156–157.
[27] W. Moffitt, *J. Am. Chem. Soc.* **1954**, *76*, 3386–3392.
[28] M. Ding, A. K. Hickey, M. Pink, J. Telser, D. L. Tierney, M. Amoza, M. Rouzières, T. J. Ozumerzifon, W. A. Hoffert, M. P. Shores, E. Ruiz, R. Clérac, J. M. Smith, *Chem. Eur. J.* **2019**, *25*, 10625–10632.
[29] L. Escalera-Moreno, J. J. Baldov, A. Gaita-Arino, E. Coronado, *Chem. Sci.* **2018**, *9*, 3265–3275.
[30] F. Neese and E. I. Solomon in *Interpretation and Calculation of Spin-Hamiltonian Parameters in Transition Metal Complexes, Vol. 4* (Eds.: J. S. Miller and M. Drillon), Wiley-VCH, Weinheim, **2003**, p. 345.
[31] S. Gomez-Coca, D. Aravena, R. Morales, E. Ruiz, *Coord. Chem. Rev.* **2015**, *289*, 379–392.
[32] S. Gómez-Coca, E. Cremades, N. Aliaga-Alcalde, E. Ruiz, *J. Am. Chem. Soc.* **2013**, *135*, 7010–7018.
[33] J. F. Hartwig, *Organotransition Metal Chemistry: from Bonding to Catalysis*, University Science Books, **2010**, p. 115.

[34] F. Aquilante, L. De Vico, N. Ferre, G. Ghigo, P. A. Malmqvist, P. Neogrady, T. B. Pedersen, M. Pitonak, M. Reiher, B. O. Roos, L. Serrano-Andres, M. Urban, V. Veryazov, R. Lindh, *J. Comput. Chem.* **2010**, *31*, 224–247.
[35] L. F. Chibotaru, L. Ungur, *J. Chem. Phys.* **2012**, *137*, 064112.
[36] F. Neese, *Wiley Interdiscip. Rev.: Comput. Mol. Sci.* **2018**, *8*, e1327.
[37] K. Ridier, A. Mondal, C. Boilleau, O. Cador, B. Gillon, G. Chaboussant, B. Le Guennic, K. Costuas, R. Lescouezec, *Angew. Chem. Int. Ed.* **2016**, *55*, 3963–3967; *Angew. Chem.* **2016**, *128*, 4031–4035.
[38] S. De, A. Flambard, D. Garnier, P. Herson, F. H. Köhler, A. Mondal, K. Costuas, B. Gillon, R. Lescouëzec, B. Le Guennic, F. Gendron, *Chem. Eur. J.* **2019**, *25*, 12120–12136.
[39] M. Atanasov, D. Aravena, E. Suturina, E. Bill, D. Maganas, F. Neese, *Coord. Chem. Rev.* **2015**, *289*, 177–214.
[40] M. J. Frisch, G. W. Trucks, H. B. Schlegel, G. E. Scuseria, M. A. Robb, J. R. Cheeseman, G. Scalmani, V. Barone, B. Mennucci, G. A. Petersson, H. Nakatsuji, M. Caricato, X. Li, H. P. Hratchian, A. F. Izmaylov, J. Bloino, G. Zheng, J. L. Sonnenberg, M. Hada, M. Ehara, K. Toyota, R. Fukuda, J. Hasegawa, M. Ishida, T. Nakajima, Y. Honda, O. Kitao, H. Nakai, T. Vreven, J. Montgomery, J. A., J. E. Peralta, F. Ogliaro, M. Bearpark, J. J. Heyd, E. Brothers, K. N. Kudin, V. N. Staroverov, R. Kobayashi, J. Normand, K. Raghavachari, A. Rendell, J. C. Burant, S. S. Iyengar, J. Tomasi, M. Cossi, N. Rega, N. J. Millam, M. Klene, J. E. Knox, J. B. Cross, V. Bakken, C. Adamo, J. Jaramillo, R. Gomperts, R. E. Stratmann, O. Yazyev, A. J. Austin, R. Cammi, C. Pomelli, J. W. Ochterski, R. L. Martin, K. Morokuma, V. G. Zakrzewski, G. A. Voth, P. Salvador, J. J. Dannenberg, S. Dapprich, A. D. Daniels, Ö. Farkas, J. B. Foresman, J. V. Ortiz, J. Cioslowski and D. J. Fox in *Gaussian 09 (Revision A.1)*, *Vol.* Wallingford, CT, **2009**.
[41] A. D. Becke, *J. Chem. Phys.* **1993**, *98*, 5648.
[42] F. Weigend, R. Ahlrichs, *Phys. Chem. Chem. Phys.* **2005**, *7*, 3297–3305.
[43] A. Schaefer, C. Huber, R. Ahlrichs, *J. Chem. Phys.* **1994**, *100*, 5829–5835.
[44] H. B. Gray, D. N. Hendrickson, Y. S. Sohn, *Inorg. Chem.* **1971**, *10*, 1559–1563.
[45] E. König, R. Schnakig, S. Kremer, B. Kanellakopulos, R. Klenze, *Chem. Phys.* **1978**, *27*, 331–344.
[46] S. Altmannshofer, E. Herdtweck, F. H. Köhler, R. Miller, R. Mölle, E.-W. Scheidt, W. Scherer, C. Train, *Chem. Eur. J.* **2008**, *14*, 8013–8024.
[47] D. Aravena, *J. Phys. Chem. Lett.* **2018**, *9*, 5327–5333.
[48] D. Reta, N. F. Chilton, *Phys. Chem. Chem. Phys.* **2019**, *21*, 23567–23575.
[49] D. Aravena, E. Ruiz, *Dalton Trans.* **2020**, *49*, 9916–9928.
[50] J. H. Van Vleck, *Phys. Rev.* **1940**, *57*, 426–447.
[51] S. S. Eaton, J. Harbridge, G. A. Rinard, G. R. Eaton, R. T. Weber, *Appl. Magn. Reson.* **2001**, *20*, 151–157.
[52] Y. S. Ding, K. X. Yu, D. Reta, F. Ortu, R. E. P. Winpenny, Y. Z. Zheng, N. F. Chilton, *Nat. Commun.* **2018**, *9*, 3134.
[53] M. Ding, G. E. Cutsail III, D. Aravena, M. Amoza, M. Rouzières, P. Dechambenoit, Y. Losovyj, M. Pink, E. Ruiz, R. Clérac, J. M. Smith, *Chem. Sci.* **2016**, *7*, 6132–6140.
[54] T. Yamabayashi, M. Atzori, L. Tesi, G. Cosquer, F. Santanni, M.-E. Boulon, E. Morra, S. Benci, R. Torre, M. Chiesa, L. Sorace, R. Sessoli, M. Yamashita, *J. Am. Chem. Soc.* **2018**, *140*, 12090–12101.
[55] M. S. Fataftah, M. D. Krzyaniak, B. Vlaisavljevich, M. R. Wasielewski, J. M. Zadrozny, D. E. Freedman, *Chem. Sci.* **2019**, *10*, 6707–6714.
[56] R. Martinez, A. Tiripicchio, *Acta Crystallogr. Sect. C* **1990**, *46*, 202–205.
[57] R. J. Webb, M. D. Lowery, Y. Shiomi, M. Sorai, R. J. Wittebort, D. N. Hendrickson, *Inorg. Chem.* **1992**, *31*, 5211–5219.
[58] S. R. Posner, L. C. Lorson, A. R. Gell, B. M. Foxman, *Cryst. Growth Des.* **2015**, *15*, 3407–3416.
[59] F. H. Allen, *Acta Crystallogr. Sect. B* **2002**, *58*, 380–388.
[60] C. R. Groom, I. J. Bruno, M. P. Lightfoot, S. C. Ward, *Acta Crystallogr. Sect. B* **2016**, *72*, 171–179.
[61] S. Alvarez, P. Alemany, D. Casanova, J. Cirera, M. Llunell, D. Avnir, *Coord. Chem. Rev.* **2005**, *249*, 1693–1708.
[62] M. Llunell, D. Casanova, J. Cirera, J. M. Bofill, P. Alemany, S. Alvarez, M. Pinsky, D. Avnir *SHAPE* 2.1., Barcelona, **2013**.
[63] P. C. Bunting, M. Atanasov, E. Damgaard-Møller, M. Perfetti, I. Crassee, M. Orlita, J. Overgaard, J. van Slageren, F. Neese, J. R. Long, *Science* **2018**, *362*, eaat7319.
[64] A. B. Buades, V. S. Arderiu, L. Maxwell, M. Amoza, D. Choquesillo-Lazarte, N. Aliaga-Alcalde, C. Viñas, F. Teixidor, E. Ruiz, *Chem. Commun.* **2019**, *55*, 3825–3828.
[65] A. Lunghi, S. Sanvito, *Sci. Adv.* **2019**, *5*, eaax7163.
[66] A. Lunghi, F. Totti, S. Sanvito, R. Sessoli, *Chem. Sci.* **2017**, *8*, 6051–6059.
[67] A. Lunghi, F. Totti, R. Sessoli, S. Sanvito, *Nat. Commun.* **2017**, *8*, 14620.
[68] L. Escalera-Moreno, N. Suaud, A. Gaita-Arino, E. Coronado, *J. Phys. Chem. Lett.* **2017**, *8*, 1695–1700.
[69] A.-M. Ariciu, D. H. Woen, D. N. Huh, L. E. Nodaraki, A. K. Kostopoulos, C. A. P. Goodwin, N. F. Chilton, E. J. L. McInnes, R. E. P. Winpenny, W. J. Evans, F. Tuna, *Nat. Commun.* **2019**, *10*, 3330.
[70] L. T. A. Ho, L. F. Chibotaru, *Phys. Rev. B* **2018**, *97*, 024427.
[71] B. L. Ramakrishna, A. K. Salzer, U. Ruppli, J. H. Ammeter, U. Koelle, *Inorg. Chem.* **1986**, *25*, 1364–1368.
[72] J. H. Ammeter, L. Zoller, J. Bachmann, P. Baltzer, E. Gamp, R. Bucher, E. Deiss, *Helv. Chim. Acta* **1981**, *64*, 1063–1082.
[73] J. H. Ammeter, N. Oswald, R. Bucher, *Helv. Chim. Acta* **1975**, *58*, 671–682.
[74] J. H. Ammeter, J. D. Swalen, *J. Chem. Phys.* **1972**, *57*, 678–698.

Manuscript received: July 18, 2021
Accepted manuscript online: September 28, 2021
Version of record online: October 27, 2021

